for accelerator meeting next week

SOME FACTORS IN HIGH INTENSITY BEAMS

W. Galbraith
D. Morgan

We attempt to set out in this paper some of the points which have to be considered when discussing the usefulness of high intensity and/or high energy proton accelerators for experimental physics. In considering the theoretically predicted particle yields, the work we have followed is that of Hagedorn[1]. So far as one has been able to test the modified Fermi statistical model in practice, there appears to be reasonable agreement between the predicted and observed yields, if by "reasonable" one does not look for better agreement than factors of 3 or 4.

The factors involved in obtaining high intensity beams relate to

a) the particle accelerating machine itself,

b) the methods for obtaining and transporting secondary beams,

and c) the experimental requirements such as spill duration and beam purity.

None of the headings should be considered independently since each is interconnected with the other but in this note we are concerned chiefly with (a). In particular, we are interested in the energy spectra of secondary particles produced in pp collisions at different incoming proton energies. In all that follows, we restrict our remarks to cyclic proton accelerators.

Machine Factors

The chief factors to be considered are the proton kinetic energy attainable and the proton intensity per pulse coupled with the pulse repetition rate.

The proton kinetic energy determines the variety of interactions which may be studied with the machine. For the purposes of this note, we take as representative energies for machines: 7 GeV, 14 GeV and 25 GeV. To compare these machines, we consider the secondary particle momentum spectra, as functions of the laboratory kinetic energy. The way in which the estimates were made is outlined in Appendix III.

The appropriate formulae giving the various centre-of-mass (CM) to laboratory transformations for a nucleon-nucleon system are given in Appendix I. The relation between CM total energy and the laboratory kinetic energy of the proton is given in Fig. 7 and some appropriate quantities calculated in Table I. Also included in another Appendix, II, is a table of laboratory threshold energies* for various reactions in pp, πp, Kp and $\bar{P}$P interactions. Thus from the momenta spectra for the various particles and the threshold information, it is a simple matter to decide the feasibility of studying a particular reaction. For example, if we wish to consider the anti-hyperons ($\bar{\Lambda}$ $\bar{\Sigma}$ $\bar{\Xi}$) we note that the thresholds in pp collisions exceed 7 GeV, and that in πp and $\bar{K}$p collisions, the thresholds exceed 4.7 and 4.9 GeV respectively. Referring to Fig. 1 it is seen that at 7 GeV the yield of π mesons of momenta greater than 5 GeV/c is very low, being right on the tail of the distributions. Similarly with K^- mesons, the yield above 5 GeV/c is almost zero, the maximum possible momentum being 6 GeV/c. [See Table I.] Evidently then to study anti-hyperons, one would have to consider energies greater than 7 GeV. How much better one might do is seen in the behaviour of the tails of the particle momentum distribution with increasing proton kinetic energy (figure 1).

*The Fermi energy of a nucleon in a nucleus will lower the threshold energy in the laboratory for the process to occur - to simplify the discussion we will neglect this. See note in Appendix IV in this connection.

In the time available, we have considered only the forward direction of emission of particles in the laboratory. Calculations of the momenta spectra at angles greater than 0° indicate a noticeable forward peaking which occurs with increasing C-M energy, as expected from the relativistic transformations.

Another feature not brought out by the separate presentation of the data in Figs. 1 - 4 is the greater effect that the C-M motion has on the momenta spectra of the Ks and $\bar{P}$s, relative to that of the π-mesons. We note this in Table I in the row marked p, the lab-momentum for maximum yield.

In Figure 5 is shown the expected behaviour of the total yield curves for π, K, $\bar{K}$ and $\bar{N}$. The form of these curves may be explained as follows. It is assumed that the threshold for production is at W_t, the total energy in the CM system, and that the cross-section rises as $(W - W_t)^{(3n-5)/2}$. It then is assumed to saturate at about $W = W_t + n M_o$, where n = number of particles in the process and M_o their rest-mass. Values of W_t, W and T_1 the laboratory kinetic energy where saturation occurs are given in Appendix III. Physically, the onset of saturation is assumed to occur when the kinetic energy of the particle corresponds to its rest mass energy in the CM system. The ~~column~~ row marked ω_+ gives the corresponding quantities for a hypothetical Boson of mass ~ 750 MeV produced in association with a Ξ (after Kaplon). If it exists and one wished to see it in reasonable intensity, this suggests that proton kinetic energies in the region 12-13 GeV should be best.

One question to ask from examination of the curves in Figs. 1 - 5 is: what is the optimum kinetic energy of the proton to produce an intense beam of particles of a given momentum? We shall consider ~~two~~ three such beams a) 500 MeV/c K^-, such as might be required for studies of K^-p capture at rest and b) a 1 GeV/c $\bar{P}$ beam and (c) a 2 GeV/c π meson beam. It should be stressed that the magnitude of the yields at low momenta depend critically upon the shape of the momentum distribution curves, and at the present time, not much weight should be put on the detailed shapes of these curves, since there is essentially no detailed experimental evidence to support them. With this warning, consider the 500 MeV/c K^- beam.

(a) 500 MeV/c K^- Beam

The predicted yields for 14 and 25 GeV collisions appear to be comparable and about a factor 2-3 times that for 7 GeV. [See Fig. 6] This suggests that an AG synchrotron, whose cycling rate at 7 GeV could be double that at 14 GeV, and a factor 4 times that at 25 GeV, would provide the most intense K^- beam operating at high repetition rate and "low" energy. It also suggests that if an AG synchrotron were operated at 1 pulse per second at 7 GeV and a "CG" machine were operated at 1 pulse every 2 seconds at the same energy, then one could predict the output K^- intensities knowing the relative proton intensities circulating in the machine*.

(b) 1 GeV/c $\bar{P}$

This beam intensity can be estimated by reference to figure 2 - note that absolute yields refer to anti-nucleons i.e. if one wishes to argue magnitude, $\bar{P}$s would be down by a factor 2. The two alternative forms of the curve for 14 GeV arise because we do not know the exact form of the CM momentum distribution at this energy. Curve I assumes a CM distribution of the same nomalised shape as at 25 GeV (from Hagedorn) and curve II that from 6.2 GeV (also from Hagedorn). The true curve clearly lies between these two extremes.

Again referring to figure 6, the absolute yields of $\bar{P}$s of 1 GeV/c is

---

*A question here refers to the possibility of multiple traversals through a target in A.G. and "C.G." machines. We note that with conventional target sizes in a "C.G." machine about 1/3 of the protons passing through would interact, thus at most multiple traversals may gain a factor ~ 2-3 in intensity.

not markedly different between 14 and 25 GeV, but the yield at 14 GeV is approximately an order of magnitude greater than at 7 GeV. [The same argument leads us to expect the yield at 7 GeV to be about an order of magnitude greater than that at 6.2 GeV; however, in this region Fermi Energy has a dominant role and when this is taken into account the factor of improvement reduces to about 5.] If the yields at 14 and 25 GeV are comparable, then there is no gain in intensity at the higher energy, if the repetition rate of the machine can be doubled when running at 14 GeV.

Regarding the π meson "contamination" in these K^- and $\bar{P}$ beams, reference to Figure 1 shows that in the former beam, the pion contamination would constitute much the same problem at 7 or 14 GeV. For the $\bar{P}$ beam, however, the $\bar{P}/\pi$ ratio increases with energy, and hence it would be advantageous to work at the higher energy.

(c) <u>2 GeV/c π meson beam</u>

Here the interest in this beam might be as a source of high momentum μ mesons or neutrinos in the 1-2 GeV/c range. In Fig. 1 it is seen that the particle yield has just reached its peak value at a laboratory momentum of 2 GeV/c for 25 GeV collisions and that at 14 and 7 GeV the intensities are down by the factors 1.7 and 4.3 respectively. Thus, again it appears that one gains significantly in going to higher proton energies, but assuming that the pulse rate of a machine at 14 GeV is twice that at 25 GeV, the total intensities attainable would appear to be about the same at these two energies and only slightly up on that possible at 7 GeV if the machine can be cycled at twice the rate at 14 GeV.

<u>Proton Intensity</u>

The figure mentioned as a desirable increase of intensity over present-day aims is a factor 100 on Nimrod. It seems unlikely that any high repetition rate A.G. machine would accept an intensity per pulse greater than that planned for this machine, say 10^{12} protons per pulse. Thus to gain a factor 100 in mean intensity, the cycling rate of the machine would have to be 50 pulses per second and involve a resonating system of magnet inductance and condensers. The maximum rate one may hope to cycle a machine whose peak magnetic field is 14 kilo gauss is ~ 20 per second i.e. a rise-time for the half sine wave 1/40 second [c.f. Princeton-Penn machine]. Thus for the Nimrod rate of rise of magnetic field, we would have to go to a maximum field of 6000 gauss or less to achieve the cycling rate. The radius of the machine for <u>7 GeV</u> would then be 2.3 times that for Nimrod. At 50 pulses per second the rise time of the half sine wave would be ≈ 10 milli-seconds, and the duration of the spill-time of the beam on to a target is unlikely to be more than 1-2 milli-seconds at the peak of the sine wave.

This leads to two points:-

1) The spill time is reasonably short and would be adaptable to bubble chamber operation. The high repetition rate, however, would be wasted on a bubble chamber, unless the chamber could effectively be made continuously sensitive e.g. by the use of ultrasonics, or by using scintillation chambers having a suitably short dead time.

2) For counter experiments the instantaneous counting rate during the 1-2 milli-second spill would be somewhere in the region 10^{10} particles per second, if comparable solid angles ($d\Omega$) and momentum bite $\left(\frac{dp}{p}\right)$ were used, as is current practice on the Bevatron. There would be no point in going to higher intensities and retain comparable beam transport systems, since the counter systems would be unable to handle the high rates. This applies to the particular case where one wishes to <u>identify</u> the primary particles say π or p in a reaction. With the Ks or Ps it appears that a further factor of ≈ 50 over expected Nimrod intensities may be tolerated before the counter system would

start to miss events due to resolving time losses. This brings in the need for excellent particle separation, since the π-meson intensity already exceeds the comfortable limit for counters. Thus to summarise the argument, if one wishes to <u>identify</u> the incoming particle in an interaction, the higher intensity would force one to reduce d and $\frac{dp}{p}$. It seems likely that one could justify going to very small $\frac{dp}{p}$ to look for cusps in cross-sections.

If one does <u>not</u> need to identify the incoming particle then an increase of intensity can be accepted, provided that sufficient purity of beam is obtained in the transport system. Here are two conflicting requirements:

a) a need for a large $d\Omega$ and $\frac{dp}{p}$ to give high intensities,

and b) a need for a small $d\Omega$ and $\frac{dp}{p}$ to achieve good particle separation.

The implications of these requirements need more thought, because it is not clear yet how good a separation and intensity may be achieved and one has to be sacrificed for the other. Current "pure" beams for bubble chambers achieve at best a 1:1 wanted particle: background condition, where the background particles are mostly μ-mesons with $\approx 10\%$ π mesons. Hence, provided that incoming particle identity is not required, more intensity in beams is advantageous. Some experiments where more <u>intensity</u> would be desired are:

1) Nucleon-nucleon scattering experiments.

2) Studies of hyperon decays, particularly the polarisation of the nucleon.

3) The leptonic decay modes of hyperons and a search for those forbidden by the $\Delta I = \frac{1}{2}$.

4) The production of neutral Ks to study the decay modes of the long-lived K_2^0.

Coupled with the study of anti-hyperons, the need for more intensity is linked with the need for higher energies.

To summarise: the more obvious advantages of increasing the primary energy of a machine appear to be:

a) there is an overall increase of fluxes of all particles, including passage over new thresholds for production,

b) the secondaries produced in the proton collisions have higher maximum energies; this is particularly important where high energy π-mesons may be required to produce further particles. It is also important since the increase in γ leads to an increase in the mean distance ($\beta\gamma c\tau$) travelled by very short-lived particles,

c) there is the possible greater production of particles at lower momenta.

<u>Other factors</u>

We list other factors which have to be taken into consideration in obtaining intense beams of secondary particles. No discussion of these is attempted in this paper.

1. Target material, size and thickness in beam direction.

2. Momentum bite (dp/p).

3. Solid angle of beam accepted into transport system.

4. For decaying particles, the length of transport system from target to detector.

5. Spill duration, especially if short $\ll$ 1 millisecond.

6. Purity of beam.

Some data relevant to target materials is tabulated in Appendix V.

In Figure 8 are curves to determine the loss of intensity of π and K mesons as a function of S/p, where S is the flight path (in metres) from target to detector and p is the momentum (in GeV/c).

<u>References</u>

1) F. Cerelus and R. Hagedorn, C.E.R.N. Report 7006/TH/39.
R. Hagedorn, C.E.R.N. Report 7424/TH/56.

2) D. Morgan, A.E.R.E. R/3242.

APPENDIX I

Centre-of-Mass - Laboratory Transformations

APPENDIX II

Laboratory Threshold Kinetic Energies for Particle Reactions

APPENDIX III

Total Yield of Particles as function of laboratory kinetic energy of proton

APPENDIX IV

Effect of Fermi Momentum Spread in Nucleon-Nucleus Collisions

APPENDIX V

Table of data pertinent to target materials

APPENDIX VI

Estimated Yields of Secondary Particles from Nimrod

APPENDIX VII

Note on the Method of Estimating the Particle Spectra

\- - -

APPENDIX I

Relativistic Transformations for C-M and Laboratory Systems

Consider a proton of kinetic energy T_L in the laboratory incident on a stationary proton.

Let β_c be the velocity of the C-M system of the two protons relative to the laboratory, and define

$$\gamma_c = (1 - \beta_c)^{-\frac{1}{2}}$$

Then the relations between the laboratory frame (L) and the CM frame (c) are as follows:

$$\beta_c = \left(\frac{\gamma_L - 1}{\gamma_L + 1}\right)^{1/2} \qquad (1)$$

$$\gamma_c = \left(\frac{\gamma_L + 1}{2}\right)^{1/2} \qquad (2)$$

$$\beta_c \gamma_c = \left(\frac{\gamma_L - 1}{2}\right)^{1/2} \qquad (3)$$

where $$\gamma_L = \frac{W_L}{M_o c^2} = \frac{T_L + M_o c^2}{M_o c^2} = 1 + T_L / M_o c^2 \qquad (4)$$

Mo being the rest mass of the proton.

We are usually concerned with the emission of a particle in the C M frame at some angle θ_c with respect to the direction of the incoming proton and at a momentum p_c in the CM frame. In the laboratory the corresponding angle of emission θ_L will be given by

$$\tan \theta_L = \frac{\sin \theta_c}{\gamma_c (\cos \theta_c + \beta_c / \beta_{cp})} \qquad (5)$$

Where β_{cp} is the velocity of the emitted particle in the C M system.

The corresponding momentum and energy would transform according to the matrix relationship

$$\begin{pmatrix} p_L \cos \theta_L \\ W_L \end{pmatrix} \equiv \begin{pmatrix} \gamma_c & \beta_c \gamma_c \\ \beta_c \gamma_c & \gamma_c \end{pmatrix} \begin{pmatrix} p_{cp} \cos \theta_c \\ W_{cp} \end{pmatrix} \qquad (6)$$

where p_{cp} = C M momentum of the emitted particle

and W_{cp} is its C M total energy. The subscripts denote corresponding laboratory quantities.

Multiplying out the matrix elements we have

$$p_L \cos \theta_L = \gamma_c \left[p_{cp} \cos \theta_c + \beta_c W_{cp} \right] \qquad (7)$$

$$W_L = \gamma_c \left[\beta_c p_{cp} \cos \theta_c + W_{cp} \right] \qquad (8)$$

For the particular case $\theta_c = \theta_L = 0$, these equations reduce to

$$p_L = \gamma_c \left[p_{cp} + \beta_c . W_{cp} \right] \qquad (9)$$

$$W_L = \gamma_c \left[\beta_c \, p_{cp} + W_{cp} \right] \qquad (10)$$

The general relations for energies in the laboratory and C M system for any two colliding particles of rest masses M_1 and M_2 (M_2 assumed at rest) are:

$$W_c = \left[(M_1 + M_2)^2 + 2 \, T_L \, M_2 \right]^{\frac{1}{2}} \qquad (11)$$

where W_c = total energy in the C M system

and T_L = laboratory kinetic energy of incoming particle of mass M_1.

Note: M_1 and M_2 are expressed in MeV in equation (11)

Then

$$\gamma_c = (T_L + M_1 + M_2)/W_c \qquad (12)$$

and $$\beta_c \gamma_c = \left[T_L \, (T_L + 2 \, M_1) \right]^{\frac{1}{2}} / W_c \qquad (13)$$

If we substitute for W_c from equation (11) and let $M_1 = M_2 = M_o$ equation (13) reduces to the form of (2).

For highly relativistic systems such as we discuss, certain approximate deductions can be made from the general formulae given above. These follow from the circumstance that the C.M. velocity of most of the particles emitted is less than the velocity of the C.M. (i.e. at 7 Gev, π's can be emitted backwards in the lab. but very few are). Thus we have

$$\langle \beta_{cp} \rangle < \beta_c$$

As a result, most particles are emitted into a cone around the forward direction and from equation (5) above, we see that approximately

$$\langle \theta_L \rangle \propto \frac{1}{\beta_c \gamma_c} \qquad (14)$$

There is therefore a progressive narrowing of the cone of emission with increasing primary energy.

We also note that, whereas the maximum possible laboratory momentum is approximately equal to that of the primary particle

$$p_L(max) \simeq W_L \qquad (15)$$

the laboratory momentum corresponding to a particular C.M. momentum increases only proportional to γ_c which itself is proportional to $\sqrt{W_{lab}}$. Since C.M. spectra tend to cluster around certain energies independent of the incoming particle energy, this means that the values of secondary particle momentum for peak emission tend to increase as $\sqrt{W_{lab}}$.

$$\langle p_L \rangle \propto \sqrt{W_L} \qquad (16)$$

These very rough considerations are brought out in the following table I. This lists γ_c , β_c and W_c, the total C.M. energy corresponding to the three values of T_L , the laboratory kinetic energy, which we have considered. It also lists for, in turn, π 's, K's, and $\bar{N}$'s the maximum possible lab. momentum p max. the most probable $\hat{p}$ and that value for which the probability is 1/20 of the maximum $p_{0.05}$. Finally, as an indication of the narrowing down of the cone of emission the ratio $R_{10^o} \equiv \frac{d^2\sigma}{dp\,d\Omega}$ (Lab Max 10^o) / $\frac{d^2\sigma}{dp\,d\Omega}$ (Lab Max 0^o) is shown for each case.

TABLE I

T_L	GeV	7.0	14.0	25.0
γ_c		2.175	2.909	3.785
β_c		0.888	0.939	0.965
W_c	GeV	4.081	5.458	7.102
p max (π)	GeV/c	6.6	13.6	24.6
p max (K)	"	6.0	13.2	24.2
p max ($\bar{N}$)	"	4.7 ≠	11.1	22.2
$\hat{p}$ (π)	"	1.1	1.5	2.0
$\hat{p}$ (K)	"	1.5	3.5	4.0
$\hat{p}$ ($\bar{N}$)	"	2.2	(4.0-5.0)	6.0
$p_{0.05}$ (π)	"	5.4	7.3	10.8
$p_{0.05}$ (K)	"	5.7	9.4	13.4
$p_{0.05}$ ($\bar{N}$)	"	4.5	(7.7-10.5)	14.8
R_{10^o} (π)		0.9	0.86	0.66
R_{10^o} (K)		0.9	0.76	0.63
R_{10^o} ($\bar{N}$)		0.7	(0.6-0.7)	0.53

≠ Results on $\bar{N}$ at 7 GeV come from calculations in which effects of Fermi momentum were included.

APPENDIX II

(after Beasley and Holliday Nuovo Cim.
1958 Supplement Vol.7 Series 10
77-90)

Laboratory Threshold Kinetic Energy in GeV for processes indicated in nucleon-nucleon collisions - N denotes nucleon.

Reaction Product	Threshold GeV.	Reaction Product	Threshold GeV.
$2N + \pi$	0.29	$2K + \Lambda^{o} + \Sigma$	3.88
$2N + 2\pi$	0.59	$2K + 2\Sigma$	4.15
$N + \Lambda^{o} + K$	1.58	$3N + \bar{N}$	5.63
$N + \Sigma + K$	1.78	$2N + \Lambda + \bar{\Lambda}$	7.10
$N + \Lambda^{o} + K + \pi$	1.96	$2N + \Lambda + \bar{\Sigma}$	7.43
$N + \Sigma + K + \pi$	2.17	$2N + \Sigma + \bar{\Lambda}$	7.43
$2N + K + \bar{K}$	2.49	$2N + \Sigma + \bar{\Sigma}$	7.76
$2\Lambda^{o} + 2K$	3.63	$N + 2\Lambda^{o} + \bar{\Xi}$	8.9
$N + 2K + \Xi$	3.73	$2N + \Xi + \bar{\Xi}$	9.0

Laboratory Threshold Energy (GeV) for processes indicated in π N collisions

Products	Threshold GeV.
$K + \Lambda^{o}$	0.76
$K + \Sigma$	0.89
$N + K + \bar{K}$	1.36
$2K + \Xi$	2.20
$2N + \bar{N}$	3.61
$N + \Lambda + \bar{\Lambda}$	4.73
$N + \Lambda^{o} + \bar{\Sigma}$	4.98
$N + \Sigma + \bar{\Sigma}$	5.24
$2\Lambda^{o} + \bar{\Xi}$	6.10
$N + \Xi + \bar{\Xi}$	6.21
$\Lambda + \Sigma + \bar{\Xi}$	6.38
$2\Sigma + \Xi$	6.67

Laboratory Tresholds (GeV) for processes indicated in

$\bar{K}$ N collisions

Products	Threshold GeV	Kinetic energy	Products	Threshold GeV	Kinetic energy
$\Lambda^0 + \pi$	< 0		$\Sigma + K + \bar{K}$	1.43	
$\Sigma + \pi$	< 0		$N + \Lambda^0 + \bar{N}$	3.68	
$\Xi + K$	0.66		$\Sigma + N + \bar{N}$	3.92	
$\Lambda^0 + 2\pi$	< 0		$N + \Xi + \bar{\Lambda}$	4.97	
$\Sigma + 2\pi$	< 0		$\Lambda + \bar{\Lambda} + \Sigma$	5.13	
$\bar{K} + N + \pi$	0.22		$N + \Xi + \bar{\Sigma}$	5.24	
$\Xi + K + \pi$	0.93		$2\Sigma + \bar{\Sigma}$	5.68	
$\Lambda^0 + K + \bar{K}$	1.26		$\Lambda + \Xi + \bar{\Xi}$	6.42	
			$\Sigma + \Xi + \bar{\Xi}$	6.72	

Laboratory Thresholds (GeV) for processes indicated in anti-nucleon nucleon collisions

Reaction Products	Threshold GeV	Kinetic energy $T_{\bar{N}}$	Reaction Products	Threshold GeV	Kinetic energy $T_{\bar{N}}$
$\Lambda + \bar{\Lambda}$	0.77		$\Sigma + \bar{\Sigma}$	1.13	
$\Sigma + \bar{\Lambda}$	0.95		$\Xi + \bar{\Xi}$	1.84	
$\Lambda + \bar{\Sigma}$	0.95		$\Lambda + \bar{N} + K$	1.58	
			$2K + 2\bar{K}$	0.19	

APPENDIX III

Total Yield of Particles as Function of Laboratory

Kinetic Energy of Protons

From Appendix I, we have

$$T_L \longrightarrow \quad Wc = \sqrt{2T_L M_o + M_o^2} \qquad (i)$$

Lab. kinetic energy — Total C.M. energy (including rest energy)

In any process, production begins at the threshold W_t and, in general, rises as $(W-W_t)^{(3n-5)/2}$ where n is the total number of products. (Special angular momentum selection rules could alter this). The sharp rise in yield above threshold may be expected to flatten off when the wavelenghts, corresponding to particle ~~movement~~ momentum, become comparable with the dimensions of the interaction volume. We assume an approximate equipartition of kinetic energy and therefore

$$W_1 = W_t + n\, M_o \quad (2) \quad (M_o = \text{rest mass of particle in question})$$

as an approximate figure for the C.M. energy at which the increase of the process flattens off

Table - all energies in GeV

	W_t	W_1	T_o	T_i
π	2.016	2.435	0.290	1.28
k	2.548	4.030	1.583	6.78
$\bar{k}$	2.864	4.84	2.49	10.61
w_+	3.01	5.26	2.94	12.85
$\bar{N}$	3.75	7.51	5.63	28.15

Symbols W_t = total C.M. energy at threshold

W_1 = total C.M. energy for flattening off

T_t and T_1 are the lab. energies of the incident proton corresponding to W_t and W_1

+ Hypothetical Particle of Mass 750 MeV produced in association with Ξ (after Kaplon)

APPENDIX IV

Effect of Fermi Momentum on C-M Motion

We give a brief discussion of the effect of Fermi Momentum of the target nucleon. This has been omitted throughout the above discussion. It will be seen that for most processes the effects are small.

We have previously given the formula

$$W_o^2 = 2\,TM + 4\,M^2 \qquad (1) \qquad \begin{cases} T = \text{lab. kinetic energy} \\ M = \text{mass of proton} \end{cases}$$

only now we write W_o for C.M. total energy, since this is for the case of zero Fermi momentum. For the case where the target particle has momentum p_2, this should be amended to read

$$W^2 \simeq W_o^2 - 2\,p \cdot p_2 \qquad (2)$$

Here p is the lab. momentum and we work to first approximation keeping only terms linear in p_2. In that case, only the component of p parallel to p is effective. We therefore have

$$W \simeq W_o\left(1 - \frac{p p_2}{W_o^2}\right) \qquad (3)$$

Using,

$$p = \sqrt{T^2 + 2\,T\,M} \qquad (4)$$

we re-write (3) as

$$W \simeq W_o\left(1 - \sqrt{\frac{T}{T + 2M}}\;\frac{p_2}{2M}\right)$$

or

$$W \simeq W_o\left(1 - \beta_{co}\,\frac{p_2}{2M}\right) \qquad (5)$$

From this it follows that

$$\gamma_c = \frac{T + 2\,M}{W} = \gamma_{co}\left(1 + \beta_{co}\,\frac{p_2}{2M}\right) \qquad (6)$$

The Fermi momentum p_2 is usually taken ~ 0.2 Gev/c. Hence, the effect is to produce changes in γ_c and W_c of the order of 10%.

Such changes are obviously significant near to threshold for processes (e.g. in $\bar{N}$ production up to about 8 GeV). They also bear on the problem of producing particles of very low or high lab. energy. Otherwise, they may be disregarded.

APPENDIX V

TABLE OF DATA PERTINENT TO TARGET MATERIALS

Mev per g.

Substance	A	Z	Density	λ_a in g	λ_t in g	X_o in g	$\frac{dE}{dx}$ (3 GeV)	$\frac{dE}{dx}$ (7 GeV)	$\frac{dE}{dx}$ (12 GeV)	$\frac{dE}{dx}$ (25 GeV)
Be	9	4	1.8	76.3	41.3	84.6	1.54	1.49	1.61	1.79
C	12	6	1.88 } 2.25 }	84.0	45.4	52	1.69	1.61	1.74	1.95
Al	27	13	2.7	110.0	59.5	26.3	1.49	1.45	1.57	1.77
Cu	63.6	29	8.94	146.3	79.1	13.3	1.27	1.25	1.37	1.55
Sn	118.7	50	5.75 } 6.55 } 7.31 }	180.3	47.5	9.1	1.09	1.09	1.20	1.37
Pb	207.2	82	11.35	217	117.5	5.9	0.95	0.99	1.09	1.25
Bi	209.0	83	9.75	218	118	5.8	0.95	0.99	1.09	1.25
U	238	92	18.68	227	123	5.42	0.91	0.92	1.02	1.18

Notes (i) λ_a, λ_t are respectively mean free paths for nuclear absorption and nuclear interaction of any kind. These are assumed not to vary significantly over the range of energies of interest.

(ii) Multiple Coulomb scattering may be estimated from the formula

$$\langle \theta^2 \rangle_{av} = \left(\frac{21 \text{ Mev}}{\beta c p} \right)^2 \frac{x}{X_o}$$

Formula (i) comes from Rossi (High Energy Particles Chap. II). The quantity x is the thickness of absorber traversed in g. (this is used throughout this Appendix as an abbreviation for g cm^{-2}), X_o is the radiation length tabulated above. The angles are in general distributed in a Gaussian distribution but for very thin targets the distribution is more peaked so that $\langle \theta^2 \rangle_{av}$ exaggerates the effective spread.

(iii) The last four columns of the table give the average energy loss from ionisation at a series of energies. In considering these, one must also take account of the energy spread ("Landau effect") which is the straggle in that part of the energy loss due to the ejection of high energy electrons (delta rays). In general, for energies of 7 GeV upwards and for targets ~ 50 g. and less there is an energy spread (half width) of $\sim \frac{Z}{A} 0.71 \times \text{MeV} = \frac{1}{5}$ to $\frac{1}{4} \times \frac{(dE)}{(dx)}$ = i.e. about a 25% spread.

(iv) For <u>internal targets</u> in a synchrotron, the angular and energy spreads discussed above produced effects on the particle motion which depend on the strength of focusing.

An angular change $\langle\theta\rangle$ produces a vertical betatron oscillation of magnitude

$$\Delta z = R\langle\theta\rangle / Q_v \qquad (2)$$

where R is the radius of the synchrotron.
Q_v is the number of vertical betatron oscillations per revolution.

Similarly, an energy charge ΔE which is effectively a momentum charge Δp of the same magnitudes ($\Delta E \approx c\,\Delta p$) causes a radial shift of the synchronous orbit Δr_s given by

$$\frac{\Delta r_s}{r} = \left(\frac{p}{r} \cdot \frac{dr}{dp}\right) \frac{\Delta p}{p}$$

$$\approx \frac{1}{Q_r^2} \cdot \frac{\Delta p}{p} \qquad (3)$$

Clearly, strong focusing reduces both effects.

APPENDIX VI (BASED ON REPORT BY W. GALBRAITH TO HARWELL ACCELERATOR SYMPOSIUM 1959)

NIMROD FLUXES ASSUMING INTERNAL TARGET STRUCK WITH 5×10^{11} PROTONS PER PULSE

(OBTAINED FROM BERKELEY EXPERIMENTAL FLUXES SCALED TO ABOVE FLUX)

Reference from which Estimate made	Particle	Momentum Gev/c	$\Delta p/p$ ±	Target and length in beam direction	Angle of Emission	Approx. Solid Angle Sterads.	Particles at Target entering transport system per pulse.	$\frac{d^2\sigma}{dp d\Omega}$ mb.sterad^{-1} (GeV/c)$^{-1}$	$A^{-2/3} \frac{d^2}{dp d\Omega}$ mb.sterad^{-1} (Gev/c)$^{-1}$
Coombes et al	π^-	0.6	± 0.05	Be 15 cm.	0°	2.2×10^{-3}	4×10^6	33	7.7
Phys. Rev.		0.9	"	" "	"	1.4×10^{-3}	5×10^6	44	10.1
112, 1303		1.4	"	" "	"	$\sim 1.2 \times 10^{-3}$	5×10^6	33	7.6
Cork et al		2.2*	"	" "	"	$\sim 0.9 \times 10^{-3}$	2×10^6	11	2.6
Phys. Rev.		3.0*	"	" "	"	$\sim 0.8 \times 10^{-3}$	10^6	5	1.1
107, 248.		4.0*	"	" "	"	$\sim 0.7 \times 10^{-3}$	6×10^5	2	0.5
Kerth	π^+	0.5	± 0.05	Cu 1 cm.	0°	3×10^{-3}	4×10^6	629	39.5
UCRL 3593		"	"	" "	30°	3×10^{-3}	8×10^5	126	7.9
		"	"	" "	60°	3×10^{-3}	2×10^5	32	2.0
		"	"	" "	90°	3×10^{-3}	2×10^5	32	2.0
Coombes et al	$\overline{P}$	0.6	± 0.05	Be 15 cm.	0°	2×10^{-3}	3	2.8×10^{-5}	6.5×10^{-6}
Cork et al		0.9	"	" "	"	1.5×10^{-3}	24	2.0×10^{-4}	4.5×10^{-5}
loc. cat.		1.4	"	" "	"	1.2×10^{-3}	270	17.7×10^{-4}	40.9×10^{-5}
		2.2*	"	" "	"	0.9×10^{-3}	500	27.8×10^{-4}	64.2×10^{-5}
		3.0*	"	" "	"	0.8×10^{-3}	180	8.3×10^{-4}	19.1×10^{-5}
Murray UCRL 8269	K^-	0.45	± 0.02	Cu 9 cm.	0°	3×10^{-3}	2000	9.7×10^{-2}	6.1×10^{-3}
Coombes et al loc. cit.		0.70	± 0.05	Be 15 cm.	0°	1.8×10^{-3}	3000	2.6×10^{-2}	6.1×10^{-3}
Ticho, Good Private Communication		1.15	± 0.0125	Ta 9 cm.	0°	0.5×10^{-3}	850	23.8×10^{-2}	7.4×10^{-3}
Kerth loc. cit.	K^+	0.5	± 0.05	Cu 1 cm.	0°	3×10^{-3}	5×10^4	7.87	0.49
		"	"	" "	30°	"	2.5×10^4	3.93	0.25
		"	"	" "	60°	"	8×10^3	1.26	0.08
		"	"	" "	90°	"	7.5×10^3	1.18	0.07

*Extrapolations using theory.

FIGURE CAPTIONS

1. The laboratory momentum spectrum of pions produced in the forward direction per (GeV/c steradian) per proton collision, as a function of kinetic energy of proton.

2. The laboratory momentum spectrum of anti-nucleons produced in the forward direction per (GeV/c. sterad) per proton collision, as a function of kinetic energy of proton. Curve I at 14 GeV - assumed CM momentum distribution similar shape to that at 25 GeV. Curve II at 14 GeV - assumed CM momentum distribution similar shape to that at 6.2GeV.

3. The laboratory momentum spectrum of K mesons (not $\overline{K}$s) produced in forward direction per (GeV/c. sterad) per proton collision - as a function of kinetic energy of proton. The overlap of the 7 GeV curve with the other two indicates problem of nomalising two sets of data.

4. The laboratory momentum spectrum of $\overline{K}$ mesons produced in the forward direction per (GeV/c. sterad) per proton collision - as a function of kinetic energy of proton.

5. Total yield of secondary particles vs primary proton kinetic energy - based on hypothesis in Appendix III. Note scale factors for yields of K, $\overline{K}$ and $\overline{N}$.

6. Estimated behaviour of particle yield of given laboratory momentum vs. kinetic energy of incoming protons. Curve I - 500 MeV/c K^-
Curve II - 1 GeV/c $\overline{P}$

7. Relation between CM total energy and the laboratory kinetic energy of incoming nucleon for a nucleon-nucleon collision.

8. Intensity loss by decay of π and K mesons as a function of momentum and flight path.

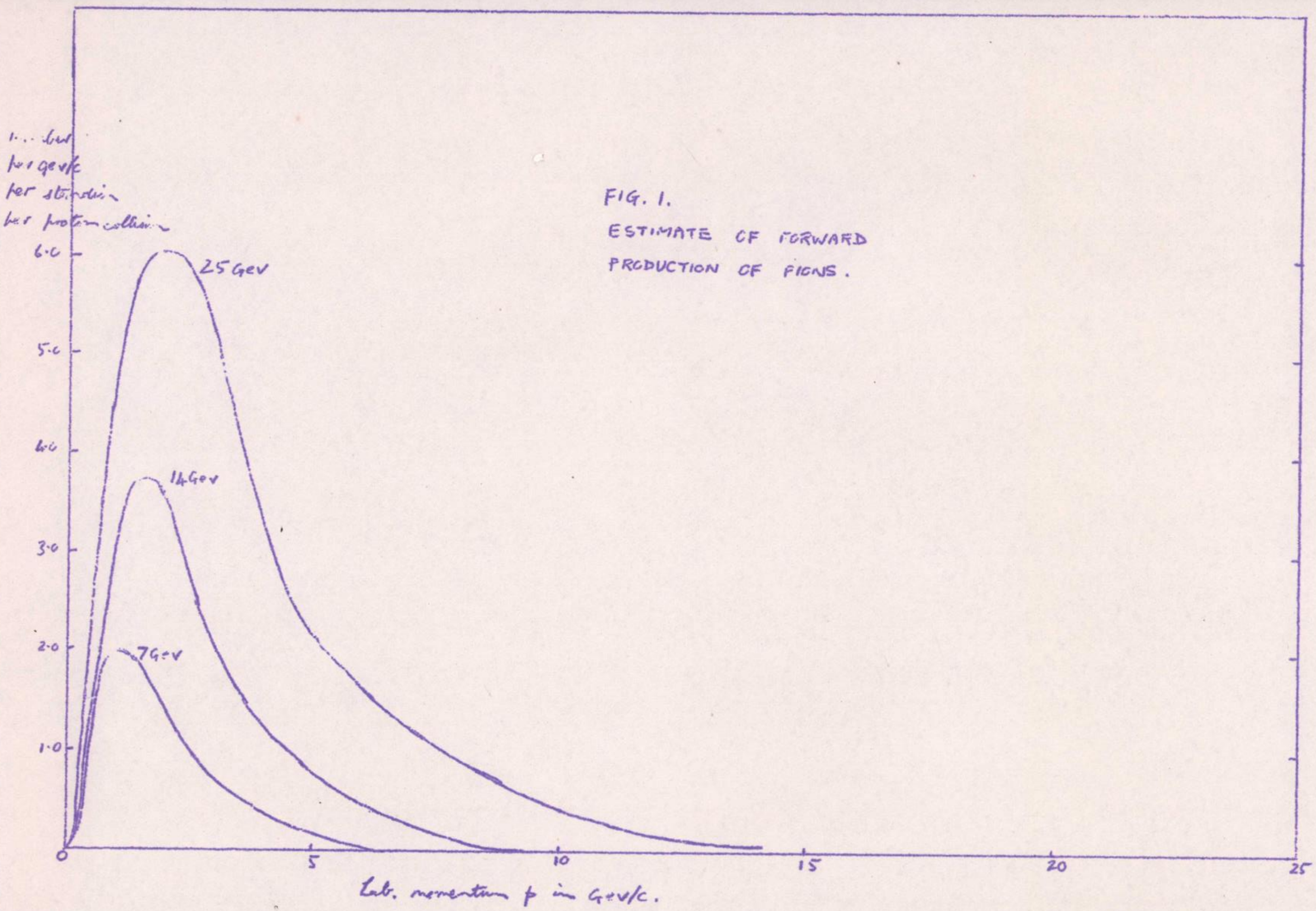

FIG. 1.
ESTIMATE OF FORWARD PRODUCTION OF PIONS.

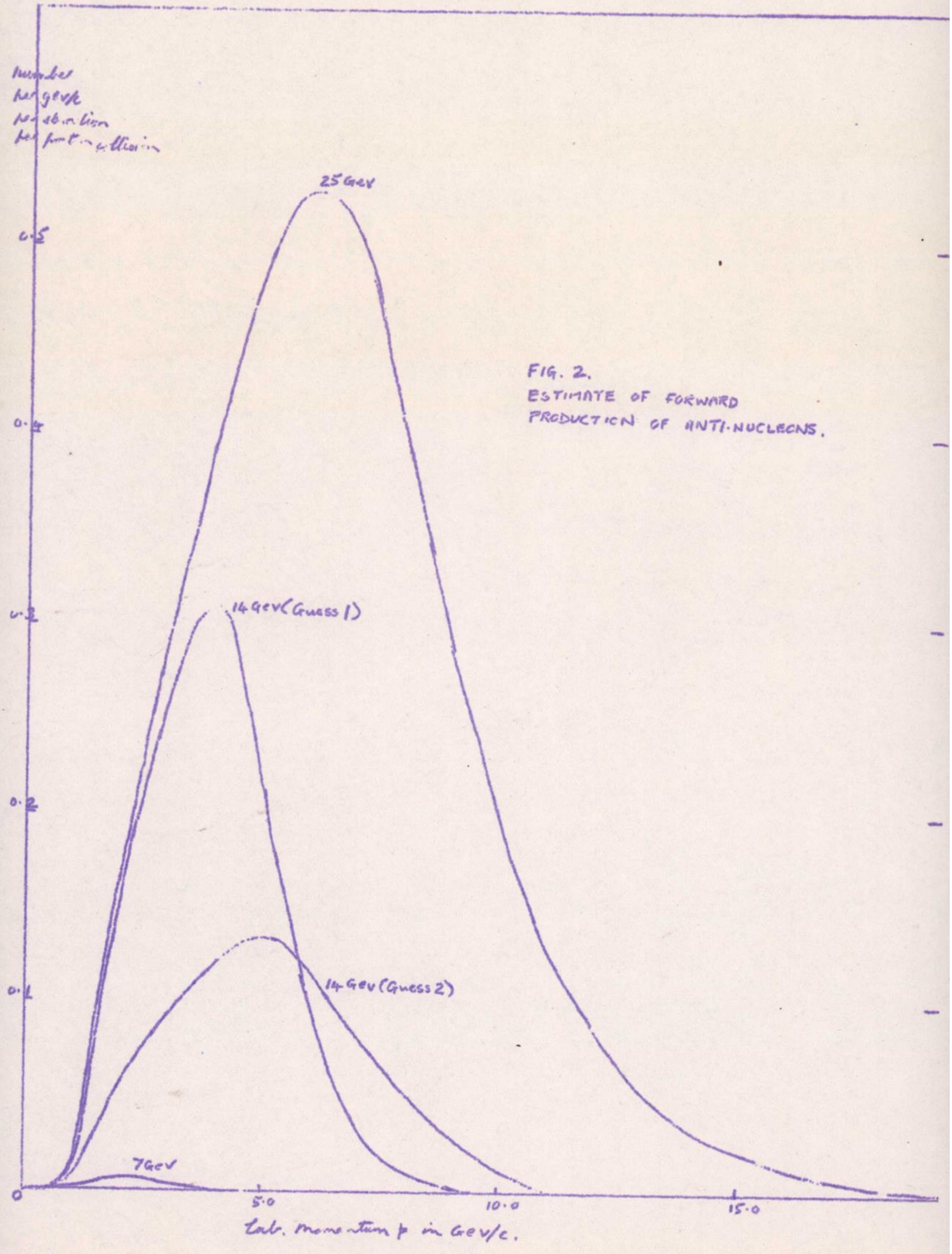

FIG. 2.
ESTIMATE OF FORWARD PRODUCTION OF ANTI-NUCLEONS.

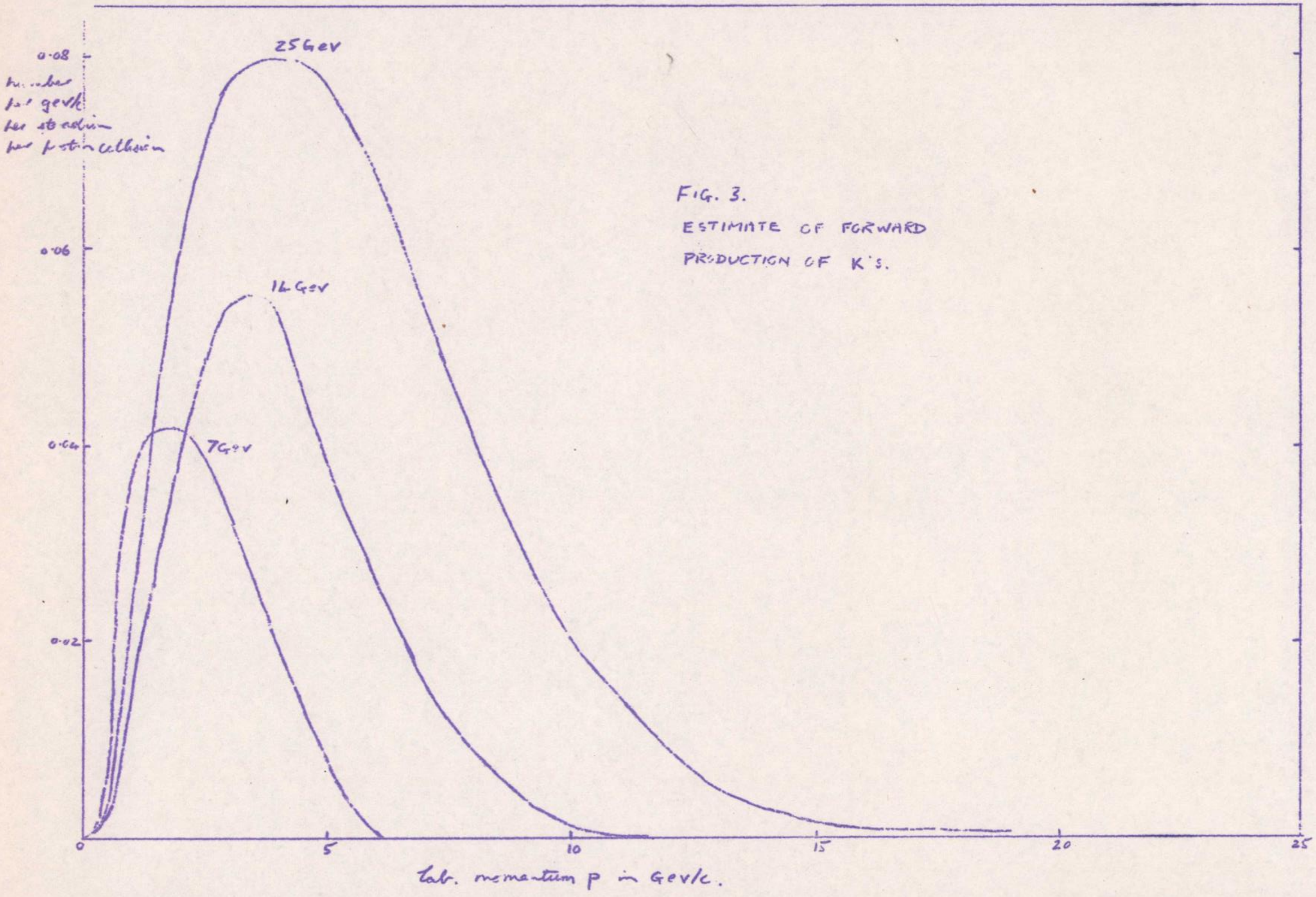

FIG. 3.
ESTIMATE OF FORWARD
PRODUCTION OF K's.

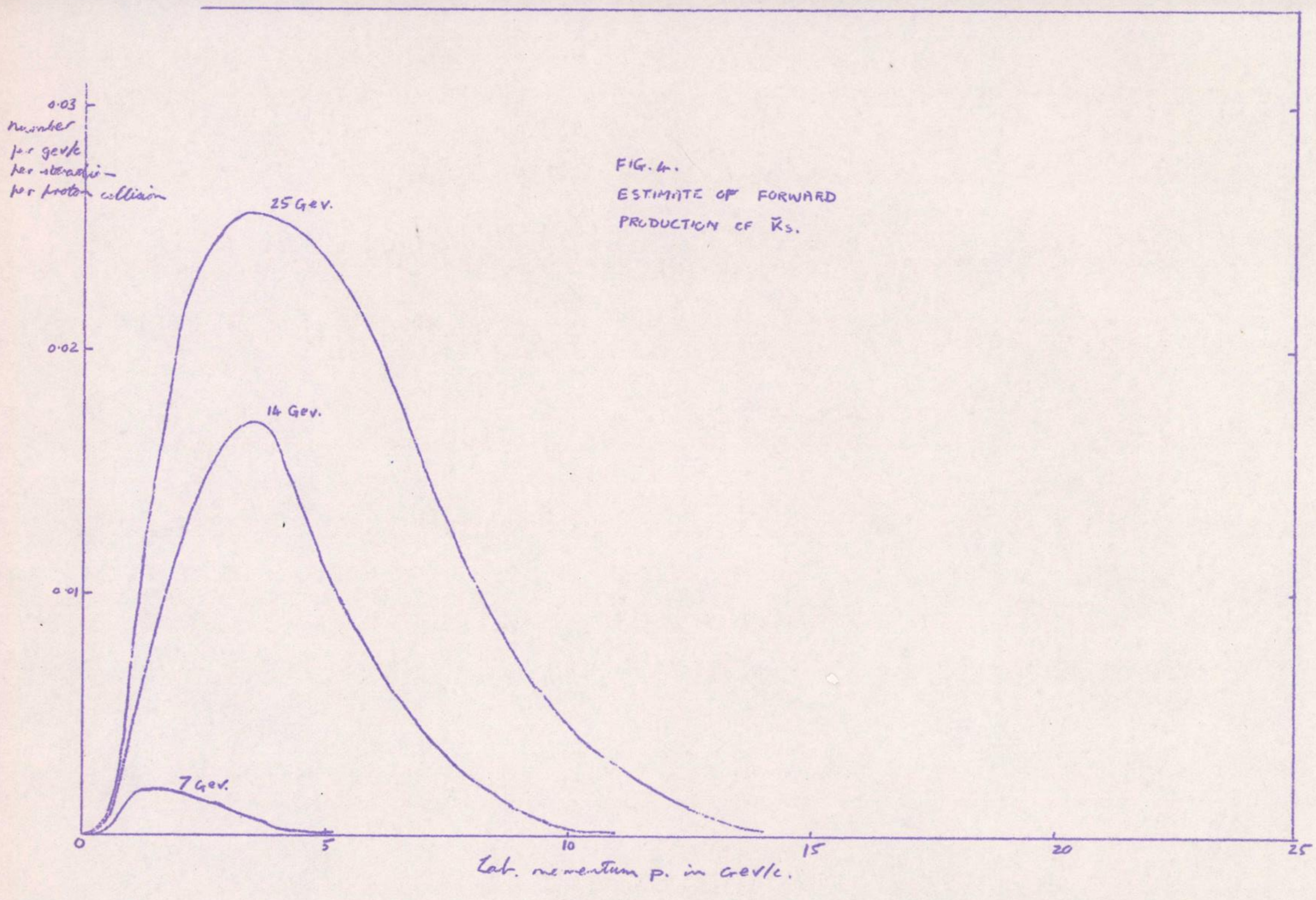

FIG. 4.
ESTIMATE OF FORWARD
PRODUCTION OF $\bar{K}$s.

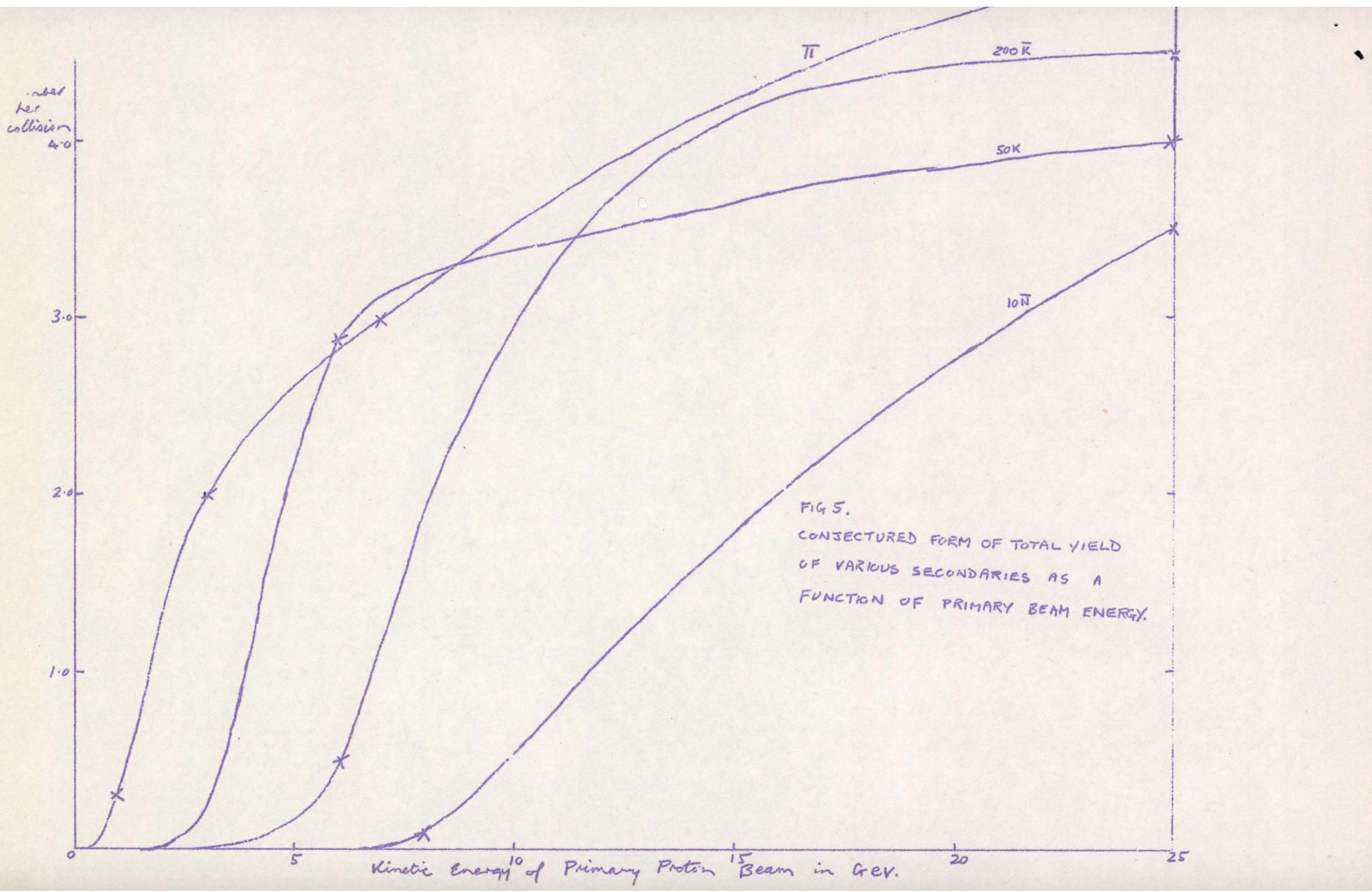

FIG 5.
CONJECTURED FORM OF TOTAL YIELD OF VARIOUS SECONDARIES AS A FUNCTION OF PRIMARY BEAM ENERGY.

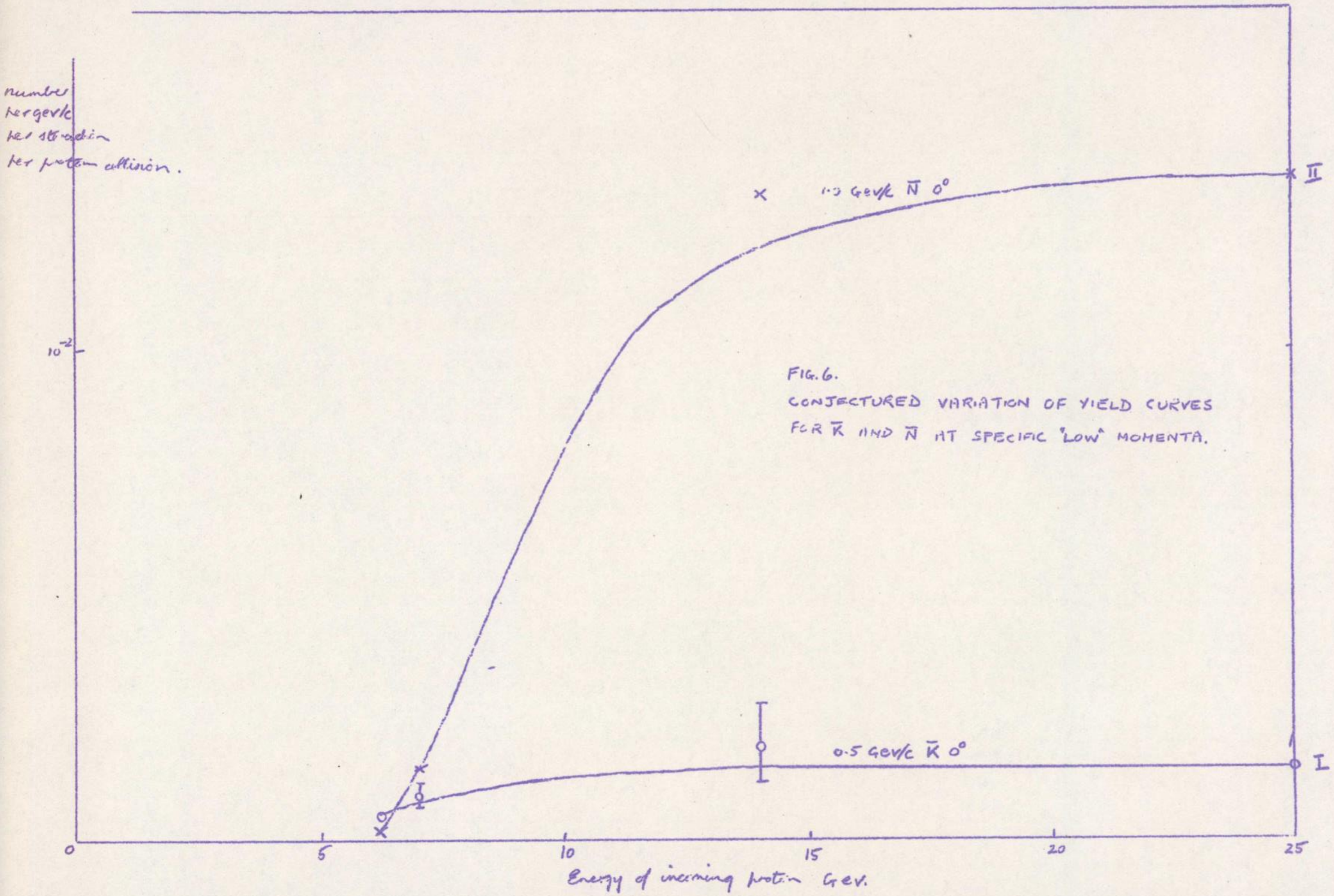

FIG. 6.
CONJECTURED VARIATION OF YIELD CURVES
FOR $\bar{K}$ AND $\bar{N}$ AT SPECIFIC 'LOW' MOMENTA.

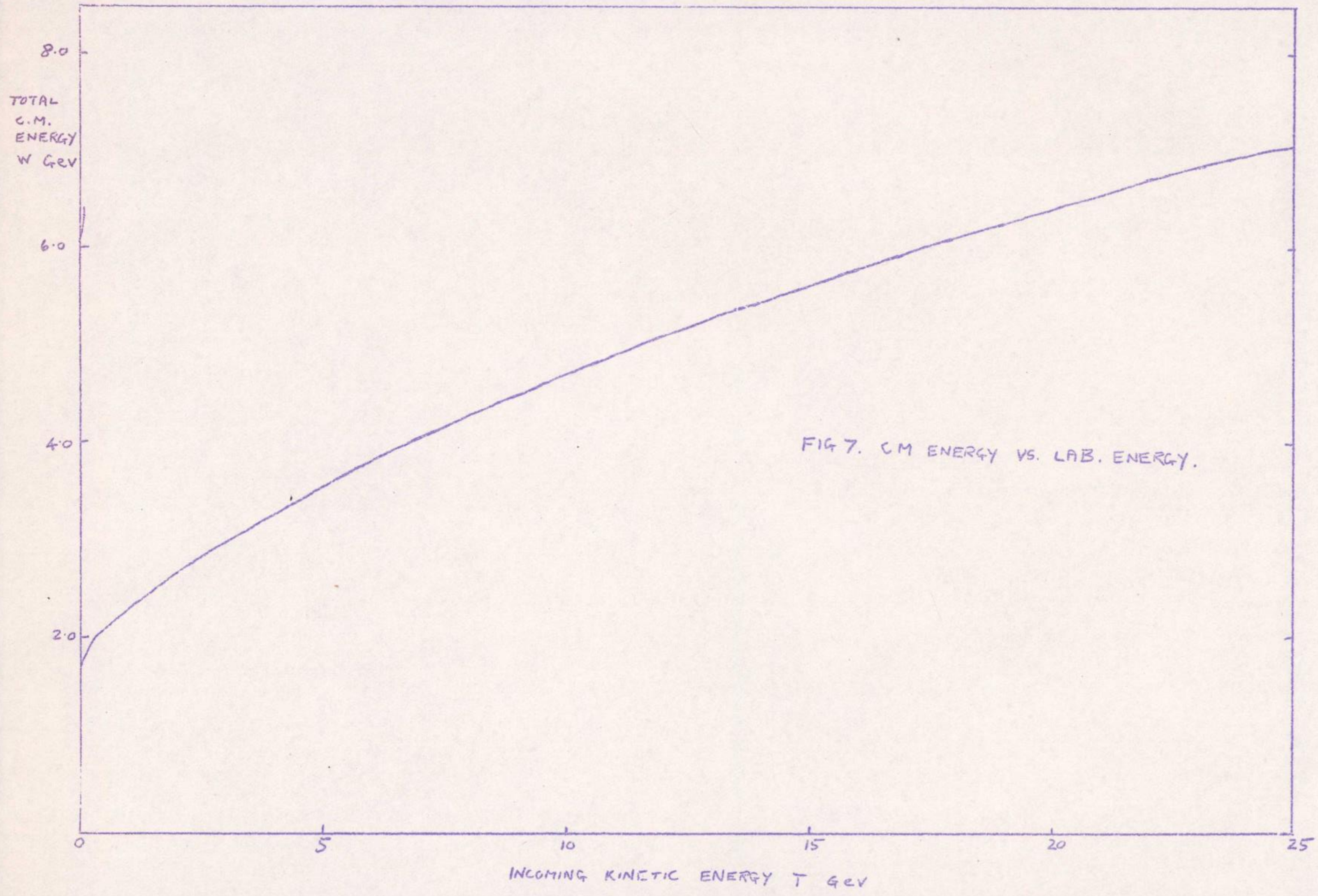

FIG 7. CM ENERGY VS. LAB. ENERGY.

FIG. 8. DECAY IN FLIGHT π AND K MESONS.